

Non-adiabatic quantum control of valley states in silicon

Alan Gardin^{1,*}, Ross D. Monaghan¹, Rajib Rahman², and Giuseppe C. Tettamanzi^{1†}

¹*Institute of Photonics and Advanced Sensing & School of Physics,
The University of Adelaide, Adelaide SA 5005, Australia. and*

²*School of Physics, The University of New South Wales, Sydney, NSW 2052, Australia.*

(Dated: June 21, 2022)

Non-adiabatic quantum effects have been experimentally observed in single-electron pumps operating at high frequencies. These have an undesirable effect on both the accuracy and precision of the resulting current source. However, when combined with the valley degree of freedom inherent to silicon, these unfavourable effects may be leveraged for novel qubit architectures. In this paper, we theoretically study, via numerical simulations, the non-adiabatic dynamics of an electron in a quantum dot formed by a SiGe/Si heterostructure. We find that it is possible to tune the electronic occupation probabilities of the final states by varying the voltages applied to the system. More importantly, the suppression of valley splitting at some spatial positions allows one to exchange the occupation probabilities of valley states. These findings show that, at least theoretically, electrical two-axis control of a valley qubit in a single dot is possible - providing a potential avenue for simpler implementation of silicon solid-state qubits.

I. INTRODUCTION

According to the quantum adiabatic theorem, a system initially in its ground state, and whose Hamiltonian evolves slowly in time, is expected to remain in the ground state of the instantaneous Hamiltonian. However, if the Hamiltonian varies quickly then this approximation is no longer valid and the state is best described by a superposition of eigenstates of the instantaneous Hamiltonian. This superposition of states induces spatial oscillations of the wavefunction, which are an observable manifestation of the violation of the quantum adiabatic theorem. An example of these effects is encountered in single electron pumps operating at fast pumping frequencies, where they lead to a decrease in the accuracy and precision of the pump [1]. Such fast operation of the pump gradually introduces higher energy states whose faster tunneling rates (from source to drain) will indeed affect the resulting current output. While these non-adiabatic oscillations are undesirable from a single-electron pumping perspective, they are reminiscent of Rabi oscillations exhibited in various qubit implementations. It is thus legitimate to question whether these non-adiabatic effects can be leveraged to build new qubit architectures controlled by non-adiabatic pulses.

In the work of *Yamahata et al.* [2], non-adiabatic oscillations are experimentally measured in a single-electron pump based on a silicon nanowire field effect transistor. In the same work, they present a simulation of the non-adiabatic oscillations between the electron orbitals for a one-dimensional quantum dot. They do not, however, take into account the valley degrees of freedom inherent to silicon, which will couple to the orbital states in the presence of impurities or interface roughness [3].

Hence, it may be possible, due to this valley-orbit coupling, for non-adiabatic oscillations to involve the valley states. Such a system would then exhibit characteristics similar to valley qubits based on double quantum dots, which have been shown theoretically to have better immunity to charge noise [4] [5] than charge qubits. Several experiments have shown that valley states can be advantageous in combining fast qubit manipulation with low susceptibility to charge noise [6] [7] [8], however the observed coherence time remained lower than that of spin qubits.

In this paper, we introduce a simple model of a [001] grown Si_{0.8}Ge_{0.2} heterostructure based on Boykin's tight-binding model for a strained silicon quantum well [9]. The tensile strain between the Si and SiGe layers breaks the six-fold degeneracy of bulk silicon, leading to a four-fold degeneracy (k_x and k_y valleys) raised in energy and a two-fold degeneracy (k_z valleys) lowered in energy. The latter can be further broken by interface roughness, impurities, or electric fields [10]. We consider only the two lowest k_z valley states because of the high energy gap (typically around 200 meV [3]) between them and the other k_x and k_y valley states. The non-adiabatic effects are introduced through a spatially varying time-dependent quantum dot potential with variable velocity v_{QD} which represents applied voltages. We orient the quantum dot potential along the x axis and the heterostructure growth axis with z , whilst neglecting the redundant y dimension.

In section II, we assume a perfectly grown heterostructure, such that the valley degrees of freedom are not affected by the non-adiabatic perturbation along the x axis. Using this idealized model, we observe non-adiabatic oscillations between the orbital states of the electron, similar to that of *Yamahata et al.* [2]. We find that it is possible to tune the final occupation probabilities of the states by varying the speed of the quantum dot, denoted by v_{QD} , through applied voltages only. A simplified analysis using a one-dimensional version of this model is pre-

* alan.gardin@adelaide.edu.au

† giuseppe.tettamanzi@adelaide.edu.au

sented in appendix A. In section III, we introduce valley-orbit coupling by varying the width of the z axis quantum well, effectively coupling the x axis orbital states with the z axis valleys. Even though there are many possible sources of such coupling, we choose this small miscut angle of 2° at the top interface of the SiGe/Si layers as it is typical in these devices. This experimentally feasible model illustrates that non-adiabatic oscillations can manifest not only between orbitals but also between valley states, as conjectured above. Interestingly, it is also possible to observe valley flipping, where a valley state is exchanged with the other valley state of the same orbital. We discuss the consequences of the observed phenomena for novel qubit schemes in section IV and conclude in section V.

II. IDEALIZED MODEL

A. Model definition

In this idealized model, we assume the growth axis z of our heterostructure to be perfectly orthogonal to the x axis, as shown in figure 1. In the x direction, the electron has a transverse effective mass $m_x = m_t = 0.19 m_e$. The quantum dot potential V_{QD} is a harmonic potential of angular frequency ω whose minimum follows a trajectory $\xi(t)$. Thus, the expression for the quantum dot potential is $V_{QD}(x, t) = \frac{1}{2} m_x \omega^2 (x - \xi(t))^2$. We choose ω such that we obtain an orbital level spacing $\Delta E = \hbar\omega = 1$ meV for the orbital states [2].

The evolution in time of the quantum dot position is the only source of time-dependence in the model. For simplicity, we choose a linear trajectory for $\xi(t)$. We additionally assume that for $t \leq t_0$, the harmonic potential is initially at position $x_0 = 0$ and that the electron is in the ground state. At $t = t_0$, the harmonic potential moves with constant velocity v_{QD} until $t = t_1$, at which the potential stops moving. The piecewise expression for the trajectory ξ of the harmonic potential is:

$$\xi(t) = \begin{cases} x_0 & \text{for } t \leq t_0 \\ x_0 + v_{QD}(t - t_0) & \text{for } t_0 \leq t \leq t_1 \\ x_1 & \text{for } t_1 \leq t \end{cases} \quad (1)$$

Note that the speed v_{QD} of the quantum dot is $v_{QD} = \frac{x_1 - x_0}{t_1 - t_0}$. Unless stated otherwise, in the rest of the paper, we fix the difference $t_1 - t_0$ to 2 ps and vary the parameter x_1 to reach different speeds. The Hamiltonian describing the dynamics along the x axis is

$$\mathcal{H}_x(x, t) = \frac{p_x^2}{2m_x} + V_{QD}(x, t) \quad (2)$$

and is identical for all z slices. An analytical study of this Hamiltonian, for a specific V_{QD} , is described in appendix A.

Valley effects are modeled using Boykin's tight-binding model for strained silicon quantum wells [9]. Boykin's

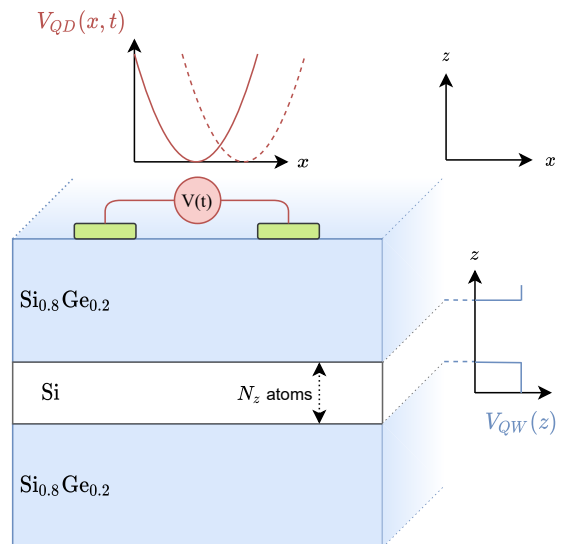


FIG. 1. Geometry of our two-dimensional SiGe heterostructure model with the y axis neglected. We apply a time-dependent harmonic quantum dot potential V_{QD} in x , and a quantum well in the z axis, originating from the SiGe/Si interfaces. The quantum well in z is composed of N_z atoms. The dashed parabola represents the potential profile at $t' > t$.

Hamiltonian for the quantum well depends on three parameters: the onsite energy ϵ , the nearest neighbor hopping v and the second-neighbor hopping u giving the Hamiltonian in equation (3).

$$\mathcal{H}_z(\epsilon, u, v) = \begin{pmatrix} \epsilon & v & u & 0 & \dots & \dots & 0 \\ v & \epsilon & v & u & 0 & \ddots & \vdots \\ u & v & \epsilon & v & u & \ddots & \vdots \\ 0 & \ddots & \ddots & \ddots & \ddots & \ddots & 0 \\ \vdots & \ddots & u & v & \epsilon & v & u \\ \vdots & \ddots & 0 & u & v & \epsilon & v \\ 0 & \dots & \dots & 0 & u & v & \epsilon \end{pmatrix} \quad (3)$$

In this Hamiltonian, each site represents an atom of the quantum well in the z axis, although this physically corresponds to a chain of atoms in the y direction we have chosen to represent this chain by a single lattice site for simplicity. We will define N_z to be the total number of atoms in the z axis, where each atom is separated by 1.366\AA . In Boykin's paper, one monolayer (ML) corresponds to two atoms, hence the number of monolayers is $N_z/2$. Note that varying the width of the Si/SiGe quantum well, as we will do in our simulations, is experimentally feasible.

The total Hamiltonian of our idealized SiGe/Si heterostructure, is the tensor product of the Hamiltonian of the x and z axis: $\mathcal{H}(x, z, t) = \mathcal{H}_x(x, t) \otimes \mathcal{H}_z(z)$. Notice that the total Hamiltonian describing the SiGe heterostructure is separable in the x and z variables, reflect-

ing the lack of coupling between the axis.

As observed in both atomistic [9] and effective mass approaches [11] to valley splitting, the final eigenstates are modulations on the atomic scale of the envelope functions $F_n(x, z)$. The lowest two valley states are the symmetric and anti-symmetric superpositions of $\pm k_0$ with $k_0 \simeq 0.82 \frac{2\pi}{a}$, where $a = 5.41 \text{ \AA}$ is the lattice spacing of the silicon crystal. We refer to these two lowest valley states by the index $v \in \{-, +\}$ in which $v = -$ is the lowest energy state and $v = +$ is the higher energy state. In our idealized model, the valley splitting is always smaller than the orbital energy spacing $\Delta E = 1 \text{ meV}$, such that the valley index $v \in \{-, +\}$ and orbital number n are good quantum numbers. Hence, in the effective mass formalism [12], the wavefunction can be expressed as:

$$\psi_{n,v}(x, z) = \sum_{j \in \{-, +\}} \alpha_j^{(v)} e^{ijk_0 z} u_j(x, z) F_n(x, z)$$

The lowest symmetric states $\psi_{n,-}$ have $\alpha_-^{(-)} = \alpha_+^{(-)} = \frac{1}{\sqrt{2}}$ leading to a cosine-like modulation of the envelope wave function F_n , while the asymmetric states $\psi_{n,+}$ have $\alpha_-^{(+)} = -\alpha_+^{(+)} = \frac{1}{\sqrt{2}}$ leading to a sine-like modulation of the envelope. We call the $\psi_{n,-}$ states the “valley down” states and the $\psi_{n,+}$ states the “valley up” states.

B. Numerical results

We numerically solve the ground state of the total Hamiltonian \mathcal{H} at the initial time and use this result as the initial wave function for solving the time-dependent Schrodinger equation. In the case of this idealized model, the ground state $\psi_{0,-}$ corresponds to a $v = -$ valley state. The resulting occupation probabilities for several values of v_{QD} are plotted below in figure 2.

Since the Hamiltonian \mathcal{H} is separable in x and z , we expect the valley degree of freedom not to influence the dynamics along the x axis. Effectively, the system behaves in time as if it was only governed by the time-evolution of \mathcal{H}_x . An analysis of this one-dimensional dynamics is described in appendix A. As a consequence, if we start the evolution in a valley down state $v = -$, the wavefunction at future times will only involve $v = -$ states. In other words, we “jump” over the $v = +$ states. This phenomenon is illustrated in figure 2, in which the occupation probabilities of the $v = +$ states are all zero as we started in a $v = -$ state. As claimed above, the results of figure 2 match those obtained by considering only the \mathcal{H}_x Hamiltonian of appendix A.

III. SMALL MISCUT ANGLE MODEL

A. Definition of the valley-orbit coupling model

In practical silicon nano-devices we always expect some degree of disorder which induces valley-orbit coupling

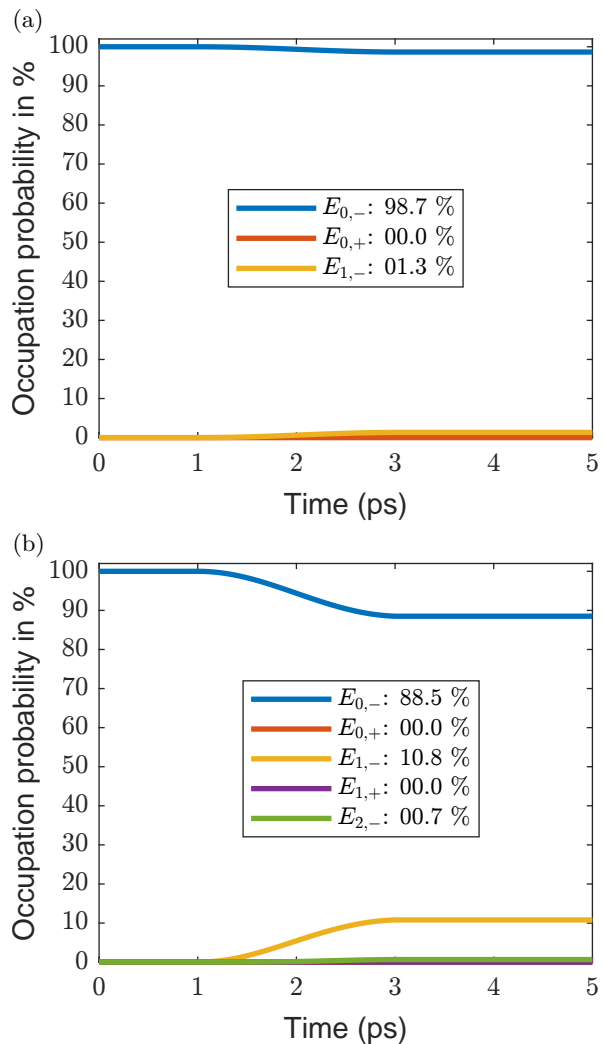


FIG. 2. Evolution of the electronic occupation probabilities for a quantum well of 6.2 nm and for (a) $v_{QD} = 2.5 \text{ nm/ps}$ (b) $v_{QD} = 7.5 \text{ nm/ps}$. Because the system is completely orthogonal, the time-dependence in the x direction does not affect the valley state occupation probabilities, hence the probabilities of the odd energy states corresponding to valley up states is zero. Note that the final occupation probabilities of the two orbital states observed here matches the simulation results of the one-dimensional model in appendix A (see figure 7). As such, the results obtained are independent of the chosen width of the quantum well. The final occupation probabilities are included in the legend.

[11]. Here, we implement disorder at the top Si/SiGe interface (strictly positive z) by having a non-constant number of atoms at different x positions. More specifically, we fix a 2° miscut angle and choose the quantum well width to be maximum (i.e N_z atoms) at the start of the x domain and have it decrease as x increases, see figure 3.

This miscut geometry introduces a dependence of the quantum well width on x , which in turn will couple the valleys with the orbitals. Note that although the miscut

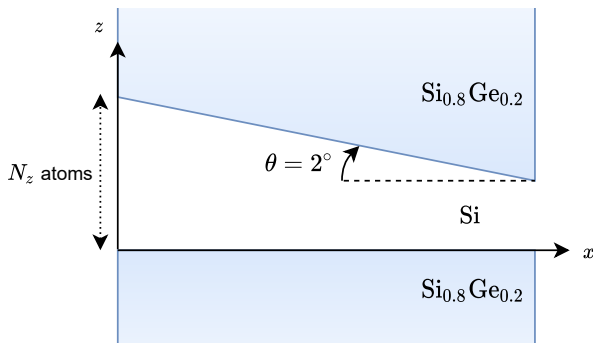


FIG. 3. Geometry of our SiGe heterostructure model with a 2° miscut. Initially, the width of the quantum well is N_z atoms and it decreases as x increases.

angle is fixed, by varying the number N_z of atoms we couple the orbitals and valleys in different ways. As a consequence, the total Hamiltonian is not separable in x and z . These interface steps have two consequences. Firstly, the energies of the wave functions will globally increase, since the electron will be confined to a smaller area. Secondly, the strength of the valley splitting, as it significantly depends on the width of the quantum well, will too be altered [13]. Again, it is important to note that the experimental feasibility of growing SiGe heterostructure of different widths, makes this an interesting model such that the numerical results presented could be easily experimentally tested.

B. Numerical results for the miscut model

We obtained a variety of results depending on the width of the quantum well and the speed of the quantum dot. We found some cases in which the 2° miscut had a minor effect on the final occupation probabilities compared to the ideal model, whereas others in which the valleys states were definitively occupied. However, the occupation of the valley states can manifest itself in several ways, as shown in figure 4.

Another interesting behavior, absent in figure 4, is that of “valley flipping”, in which the occupation of the down valley is shifted to that of the up valley while the higher orbital states remain in the valley down state (i.e the occupation of the $\psi_{0,-}$ state is transferred to the $\psi_{0,+}$ state). Valley flipping can appear for different excitations and geometries, and the degree to which this charge transfer between the valley states occurs can also vary.

In the two examples of figure 5, we only display systems in which the final wavefunction is a good two-level system. In the first case, a qubit could be encoded on the valley states of the first orbital $\psi_{0,-}$ and $\psi_{0,+}$, while in the second, the qubit could span the valley up of the first orbital $\psi_{0,+}$ and the valley down of the second orbital $\psi_{1,-}$. In this second case, one could still encode the qubit on the valley states of the first orbital by lifting the energy of the excited orbital states $\psi_{1,v}$ by an increase

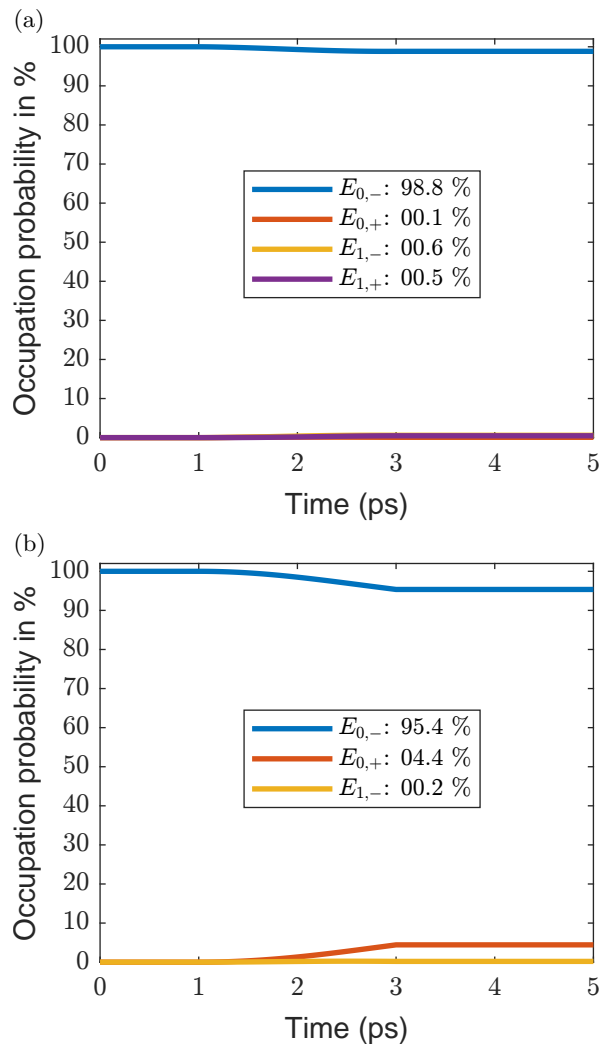


FIG. 4. Evolution of the electronic occupation probabilities for a 2° miscut and $v_{QD} = 2.5$ nm/ps. (a) For a quantum well width of 9.8 nm, the final occupation probabilities are distributed over the first two orbital states ($n \in \{0, 1\}$) and their respective valley states. (b) For a quantum well of 7.3 nm, both valley states of the first orbital are primarily occupied. Note that the excitation supplied in cases (a) and (b) is the same, the only difference being the width of the quantum well. The final occupation probabilities are included in the legend.

of the quantum dot potential V_{QD} (i.e changing the level spacing ΔE). It is also surprising to note that in the second case, the initial ground state is almost completely removed from the final wavefunction (final probability of only 0.5% for $\psi_{0,-}$).

Valley flipping is closely related to the chosen geometry and how the induced coupling influences the valley splitting. Indeed, in our study, valley flipping only occurred when an avoided crossing was present in the time evolution of the spectrum. In figure 5, the spectrum evolution in time corresponding to the two valley flipping examples is shown. We see that the smaller the gap be-

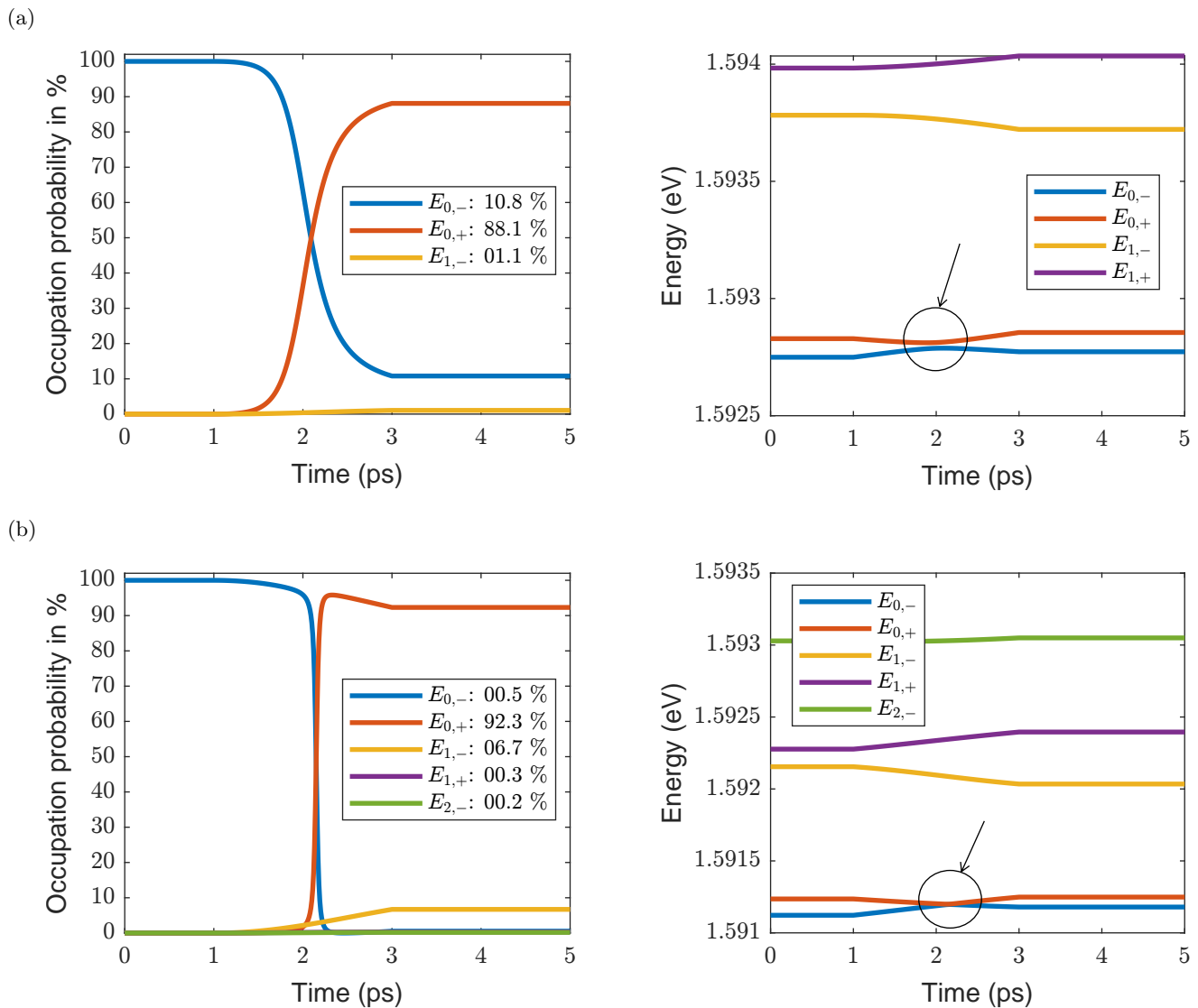


FIG. 5. Example of valley flipping behavior shown through the time-evolution of electronic occupation probabilities (left) and of the corresponding spectrum (right) for a 2° miscut angle for (a) $v_{QD} = 2.5$ nm/ps and a quantum well width of 8.1 nm (b) $v_{QD} = 5$ nm/ps and a quantum well width of 9.5 nm. In these two examples, the final system is close to a two-level system which may have implications for novel qubit schemes. In both cases, we notice an avoided crossing in the spectrum (indicated by a circle), allowing valley flipping to occur. The final occupation probabilities are included in the legend.

tween the two lowest eigenstates, the stronger the valley flipping. We also expect that the perturbation applied to the system must have sufficient energy to allow the system to cross the energy gap between the two valley states. In our model, the avoided crossing corresponds to a suppression of valley splitting. This splitting is induced by the applied quantum dot potential being centered at some specific spatial location. This phenomenon has been theoretically predicted in tight-binding models [9], with valley splitting decreasing as the width of the quantum well increases. Theoretical calculations using effective mass approaches showed similar results when considering a small miscut angle [11], which are due to

the presence of interface steps [14]. However, such valley splitting suppression can also manifest due to interface roughness [15], hence we expect that valley flipping could manifest in systems of different geometries, as long as a small energy gap exists between two states.

IV. DISCUSSION OF QUBIT APPLICATIONS

A qubit can be defined as a two-level system, i.e a system living in a two-dimensional Hilbert space. However, in the model used, the harmonic oscillator can be infinitely excited and the valley degrees of freedom mul-

multiply the availability of states by two.

Nevertheless, we note that the transition to the non-adiabatic regime is smooth and increases with the speed of the quantum dot, as observed in the plots of figure 2 and confirmed by the criterion obtained in appendix A. To obtain a good two-level system for qubit applications, the quantum dot speed should not be too fast as then higher energy states will begin to appear. Thus there exists a range of speeds for which one can smoothly tune the occupation probabilities of the ground and first excited state whilst limiting the appearance of further excited states. Moreover, the time over which this perturbation is applied can be used to tune the final occupation probabilities (see figure 6). Together, this may be used to implement a rudimentary σ_z rotation.

To make a two-axis control of such a qubit possible, it is necessary to implement not only σ_z but also σ_x rotations. In our system, valley flipping would provide a natural implementation of a σ_x rotation. Controlling this rotation amounts to controlling the valley splitting, which we cannot precisely predict in general. However, variations of the valley splitting are likely to occur in any realistic device, thus a basic implementation of such a rotation may be feasible.

Concerning the choice of computational basis, it would be desirable to use the valley states of the first orbital. Indeed, such states are similar to states used in valley qubits, and previous implementations of valley qubits in double quantum dots have shown a coherence time on the scale of nanoseconds [7] [8]. However, the qubits were implemented in double quantum dots, while our system is a single quantum dot. Still, we expect the coherence time of our architecture to have similar order of magnitude. Choosing the valley states of the first orbital as the computational basis, it is necessary to isolate them from higher orbital states. This could be implemented by tuning the quantum dot confinement potential so that increasing the orbital level spacing ΔE makes it harder for the system to transition to such states.

Under these theoretical conditions, two axis control of a qubit may be possible. One possibility would be to chain different geometries for each operation and move the state adiabatically between different geometries. In our system, all control depends on precisely manipulating both the speed and position of the quantum dot. This is performed through voltages applied to the gates on top of the SiGe heterostructure. This all-electrical control of the occupation probabilities is critical for scalability, as one would have no need for microwave lines for qubit manipulation as in most spin qubits. A second advantage is that we are not constrained by any adiabatic condition. As a consequence, provided the decoherence times are similar to that of other hybrid valley qubits, we can perform orders of magnitude more gate operations.

However, difficulties still remain. First, engineering the electrical pulses used in our simulation may be challenging because of the required time scales involved. Such high speeds are however experimentally feasible as

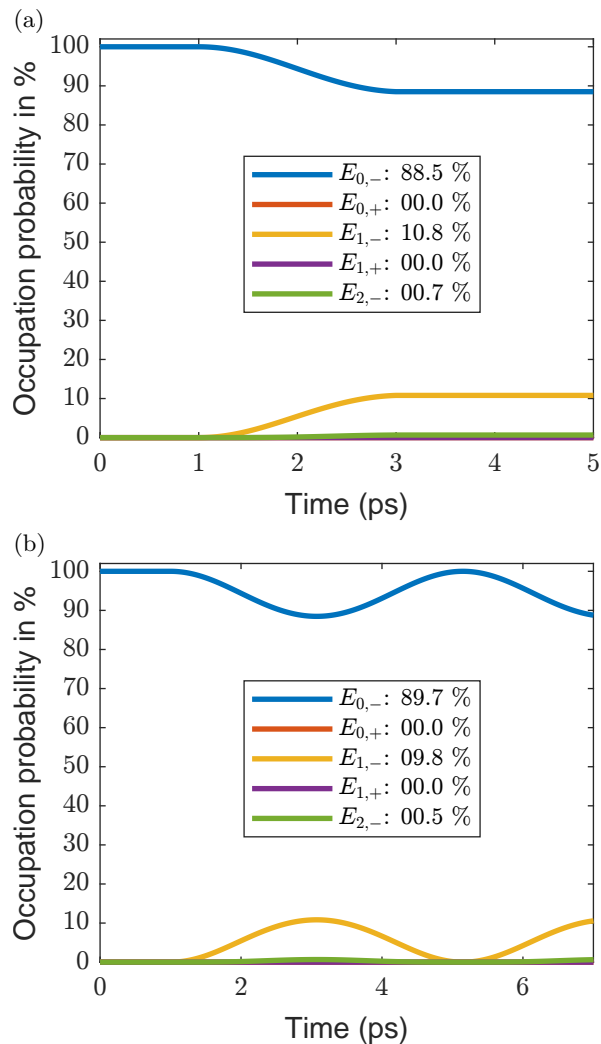


FIG. 6. Evolution of the electronic occupation probabilities of the ideal model for a quantum well of 6.2 nm and for $v_{QD} = 7.5$ nm/ps over different time scales. In both cases, the movement of the quantum dot starts at 1ps. (a) The perturbation lasts 2 ps (b) The perturbation lasts 8 ps. This illustrates that tuning the occupation probabilities is possible by varying for how long the perturbation is applied. The final occupation probabilities are included in the legend.

demonstrated in *Yamahata et al.*'s work using a 4GHz RF source. Still, it may be possible to obtain similar qubits operations with longer pulses (using our linear trajectory, we would increase the final position x_1 to reach the same values of v_{QD}). On the other hand, we have been limiting ourselves to linear trajectories, and hence more complicated trajectories are unexplored. The control of the quantum dot trajectory ξ depends on the potential profile V_{QD} of the device, which may be challenging to precisely engineer. We also note that, typically, for high quality qubits, we need the probabilities shown in the previous figures to go from 0 to 100%. This was not the case in our simulation but we expect that more fine-tuning could solve this issue. We also neglected relaxation of

inter-valley and intra-valley states. Finally, coupling to other such qubits has not been explored and may pose a significant technical challenge.

Still, this kind of control could have applications in other type of qubit systems. Indeed, we are limiting ourselves to the study of a single quantum dot and hence a single driving pulse. Hence, we suspect that the results presented in this work could be adaptable to more complicated double dot systems making the possible implementation of these ideas more realistic.

V. CONCLUSION

Our results show that by combining two conventionally undesirable effects, namely non-adiabaticity and valley splitting suppression, we can control transitions between different valley-orbit states. Non-adiabaticity stems from applying fast time-dependent voltages to our system, while valley splitting suppression originates from the spatial dependence of the energy gap between valley states. Using numerical simulations, we showed how time-dependent voltages can move an electron towards an avoided crossing in the spectrum where valley flipping can occur. This general idea can manifest in a variety of systems in which a small energy gap exists, see for instance the paper of *Campbell et al.* [16], where this is demonstrated for superconducting qubits.

Note, however, that our model is highly idealized, namely we neglected both the strain and alloy disorder of the Ge atoms, and the relaxation of intra-valley and inter-valley states. We also note that our work is only valid in the low density limit hence ignoring both Coulomb and exchange effects. Additionally, in this work we limited ourselves to linear trajectories (movement at constant speed), but more complicated perturbations could lead to finer control of the final state probabilities. A drawback of our study is that we only varied the final position x_1 to tune the speed of the quantum dot. However, due to the 2° angle miscut, this entails moving the wave function through a greater number of interface steps. Traversing a larger distance offers more possibilities for avoided crossings in the spectrum, potentially bringing more opportunities for valley flipping. Finally, the precise engineering of both the device geometry and the applied voltages for adequate control poses additional experimental challenges.

Nevertheless, non-adiabatic control of valley states may open novel quantum information processing schemes. In particular, a qubit based on this physics would be both fast and benefit from an all-electrical control, critical for scalability. As explained in section IV, one can induce electronic transitions reminiscent of elementary operations necessary for functional qubit implementations. Non-adiabatic control of qubits by exploiting the avoided crossing from valley splitting suppression could be used in other qubit schemes, such as charge qubit or hybrid qubits (valley-spin) in double quantum

dots. In this work, the spin degree of freedom has been neglected, but a hybrid spin-valley qubit could have interesting properties, namely it would benefit from the high coherence time of spin and the fast gate operation of charge qubits with a protection from charge noise. Additionally, in some emerging 2D and topological materials, spin and valleys are strongly momentum locked, thus by manipulating valleys, one could also manipulate spins non-adiabatically.

ACKNOWLEDGMENTS

This work is was partly funded under the Nicolas Baudin initiative and Thales Australia. We acknowledge useful discussions with Dr. Edyta Osika concerning alternative simulation methods. This work was supported with supercomputing resources provided by the Phoenix HPC service at the University of Adelaide. Associate Professor Rajib Rahman acknowledges support from the US Army Research Office under grant number W911NF-17-1-0202.

Appendix A: One-dimensional model without valleys

1. Model definition and preliminary results

In this section, we consider the one-dimensional dynamics of an electron in a silicon quantum dot moving spatially (along the x axis) in time, with the k_z valleys being neglected. The results of this section are applicable to a perfectly grown SiGe heterostructure like the one discussed in section II. Because of the absence of valleys, this model is similar to the one developed in *Yamahata et al.*'s original work [2].

The time-dependent Hamiltonian of our system precisely corresponds to the Hamiltonian \mathcal{H}_x (equation 2) describing the x axis in the two-dimensional model of section II. In the one-dimensional model of this section, we rewrite \mathcal{H}_{1D} as:

$$\mathcal{H}_{1D}(x, t) = \frac{p_x^2}{2m_x} + V_{QD}(x, t) \quad (\text{A1})$$

where $V_{QD}(x, t) = \frac{1}{2}m_x\omega^2(x-\xi(t))^2$ and ξ is the position of of the quantum dot potential minimum. The time evolution of the electron can be obtained by solving the one-dimensional time-dependent Schrodinger equation. Even though exact analytical results might be obtained for a time-dependent harmonic potential [17] [18], for simplicity we chose to solve this equation numerically.

The result of the simulation for three values of v_{QD} are plotted in figure 7. In the left column, we can observe spatial oscillations of the probability density, similar to the results of *Yamahata et al.* We estimate analytically (see appendix A 3 for a derivation) that above approximately $v_{QD} \approx 2.2$ nm/ps, the condition for the adiabatic

regime is broken. In this non-adiabatic regime, the wavefunction will be in a superposition of eigenstates of the instantaneous Hamiltonian. This superposition then induces a spatial oscillation as will be discussed in the next subsection. Notice from figure 7 that the greater v_{QD} , the greater the amplitude of the spatial oscillations. This dependence of the amplitude with the speed of the quantum dot is both intuitive and provable analytically (see the next subsection and the classical analogy). In the right column, we plot the evolution in time of the occupation probabilities of the orbitals by projecting the simulated wavefunction on the instantaneous basis of the harmonic oscillator at each time. Again, as intuitively expected, the greater v_{QD} , the higher the probability of excited states in the final wave function.

2. Spatial oscillations of the probability density

In this subsection, we explain the origins of the observed non-adiabatic oscillations in this 1D model. Let us assume that the system is initially in its the ground state. We know from the adiabatic theorem that if the change in the Hamiltonian is slow enough, the electron will remain in the ground state of that instantaneous Hamiltonian. In other words, the electron will be in the ground state of the harmonic oscillator centered at the minimum of the potential given by $\xi(t)$. However, if the Hamiltonian evolves in time quickly, then we expect the electron to be in a superposition of eigenstates of the instantaneous Hamiltonian. For a superposition of only two eigenstates (achievable at low v_{QD}), this behavior is reminiscent of Rabi oscillations, and will manifest in spatial oscillations of the probability density as observed in figure 7 as well as by a non-zero probability for the first excited state after a certain period of time.

We now show how a superposition of two eigenstates induces spatial oscillations of the probability density. Let us consider the time-independent Hamiltonian of a particle in a harmonic potential centered in x_0 :

$$\hat{H} = \frac{\hat{p}^2}{2m} + \frac{1}{2}m\omega^2(\hat{x}^2 - x_0)^2 \quad (\text{A2})$$

The energy levels $E_n = \hbar\omega(n + \frac{1}{2})$ of the harmonic oscillator give an even level spacing of $\Delta E = \hbar\omega$. Let us assume that the system is confined to the two lowest energy levels E_0 and $E_1 = E_0 + \Delta E$, and let us denote $|\varphi_0\rangle$ and $|\varphi_1\rangle$ as the associated eigenstates. The Hamiltonian can be written in the $\{|\varphi_0\rangle, |\varphi_1\rangle\}$ basis as :

$$\hat{H} = \begin{pmatrix} E_0 & 0 \\ 0 & E_1 \end{pmatrix} = E_0 I_2 + \begin{pmatrix} 0 & 0 \\ 0 & \Delta E \end{pmatrix}$$

where I_2 is the 2×2 identity matrix.

The time-evolution operator \hat{U} for our system is:

$$\hat{U}(t) = e^{-\frac{i}{\hbar}\hat{H}t} = e^{-\frac{i}{\hbar}E_0t} \begin{pmatrix} e^0 & 0 \\ 0 & e^{-\frac{i}{\hbar}\Delta Et} \end{pmatrix} \\ \sim \begin{pmatrix} 1 & 0 \\ 0 & e^{-\frac{i}{\hbar}\Delta Et} \end{pmatrix}$$

where we have discarded the non-observable global phase factor $e^{-\frac{i}{\hbar}E_0t}$. By defining $\tau_{\text{coh}} = \frac{2\pi\hbar}{\Delta E}$ we have:

$$\hat{U}(t) = \begin{pmatrix} 1 & 0 \\ 0 & e^{-i2\pi\frac{t}{\tau_{\text{coh}}}} \end{pmatrix}$$

Assume the state at $t = 0$ is a superposition of the ground and first excited state (for instance due to a sudden change of the Hamiltonian as discussed above) of the form:

$$|\psi(t=0)\rangle = \sqrt{1-p}|\varphi_0\rangle + \sqrt{p}|\varphi_1\rangle \sim \begin{pmatrix} \sqrt{1-p} \\ \sqrt{p} \end{pmatrix}$$

Then at time t , this state becomes:

$$|\psi(t)\rangle = \hat{U}(t)|\psi(t=0)\rangle \\ = \begin{pmatrix} 1 & 0 \\ 0 & e^{-i2\pi\frac{t}{\tau_{\text{coh}}}} \end{pmatrix} \begin{pmatrix} \sqrt{1-p} \\ \sqrt{p} \end{pmatrix} \\ \sim \sqrt{1-p}|\varphi_0\rangle + e^{-i2\pi\frac{t}{\tau_{\text{coh}}}}\sqrt{p}|\varphi_1\rangle \quad (\text{A3})$$

This equation looks similar (minus an initial phase θ) to the one claimed by *Yamahata et al.* [2]. Note that here the superposition is time-dependent but the state probability is time-independent, since p does not depend on time.

Assuming equation A3 results from the adiabatic theorem for a strong perturbation, we are now in a position to justify the spatial oscillations. The average position can be expressed as:

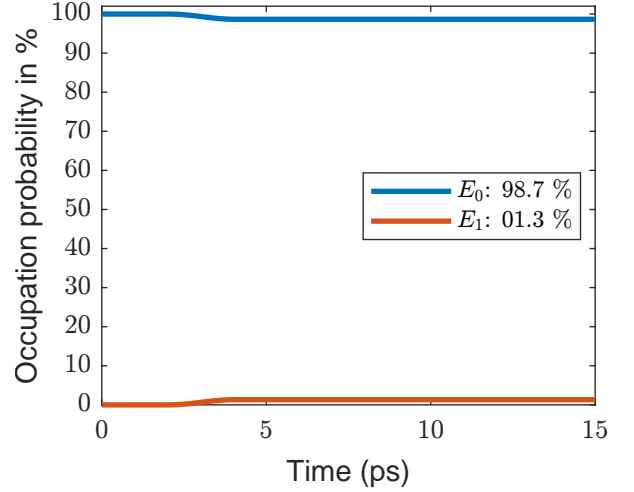
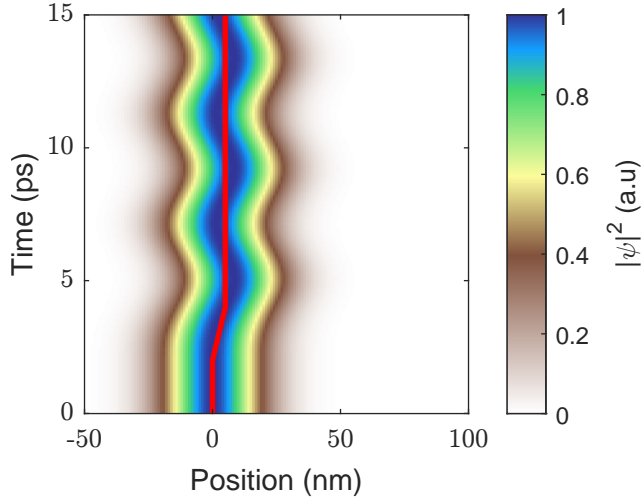
$$\langle x \rangle(t) = \langle \psi(t) | \hat{x} | \psi(t) \rangle \\ = (1-p)\langle \varphi_0 | \hat{x} | \varphi_0 \rangle + p\langle \varphi_1 | \hat{x} | \varphi_1 \rangle \\ + 2\sqrt{p(1-p)}\cos\left(2\pi\frac{t}{\tau_{\text{coh}}}\right)\text{Re}\{\langle \varphi_0 | \hat{x} | \varphi_1 \rangle\}$$

Because our Hamiltonian is assumed to be centered at x_0 (see equation A2), we have $\langle \varphi_0 | \hat{x} | \varphi_0 \rangle = \langle \varphi_1 | \hat{x} | \varphi_1 \rangle = x_0$. Furthermore, using equation (4.174) of the book by Bransden and Joachain [19], one can show that $\langle \varphi_0 | \hat{x} | \varphi_1 \rangle = \sqrt{\frac{\hbar}{2m\omega}}$. Using this, we obtain the following equation for the evolution of the average position:

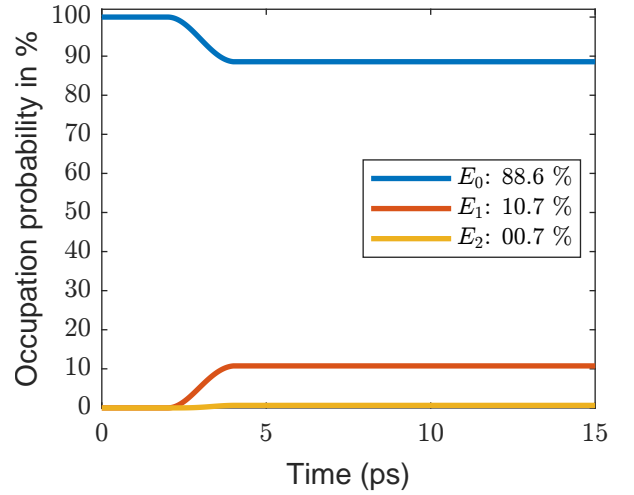
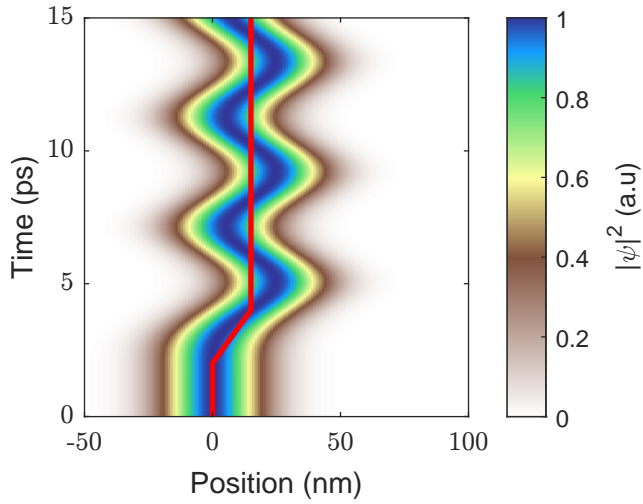
$$\langle x \rangle(t) = x_0 + \sqrt{\frac{2\hbar p(1-p)}{m\omega}}\cos\left(2\pi\frac{t}{\tau_{\text{coh}}}\right) \quad (\text{A4})$$

Hence, we see that the average position oscillates with period τ_{coh} as verified by the simulations. This is reflected in the probability density plots (left column of figure 7), where the average position is found at the center of the

(a) Quantum dot speed of 2.5 nm/ps



(b) Quantum dot speed of 7.5 nm/ps



(c) Quantum dot speed of 15 nm/ps

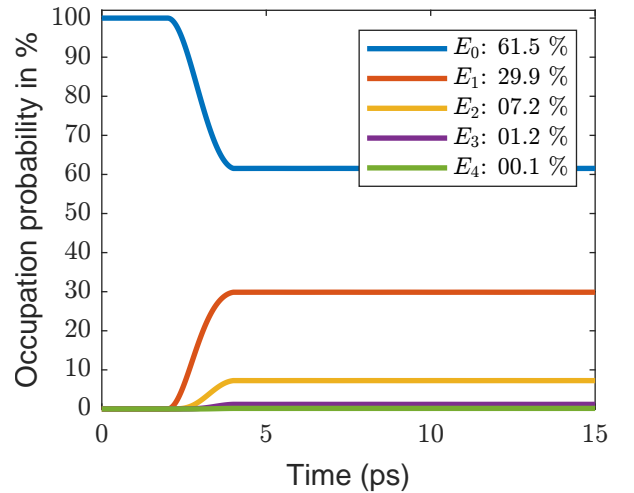
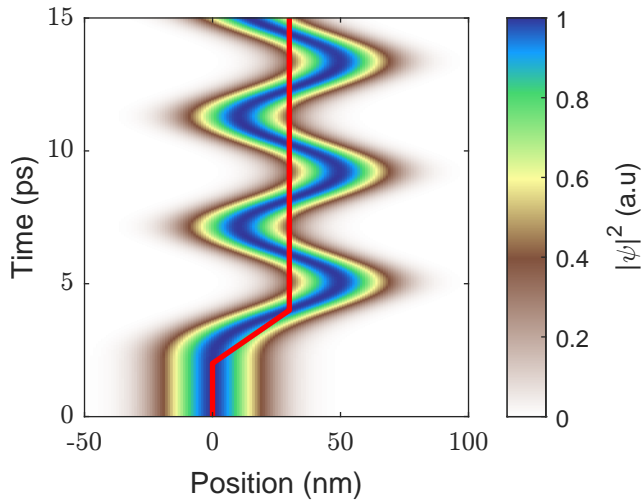


FIG. 7. Evolution of the probability density of the electron in space and time (left) and associated time-evolution of the electronic occupation probabilities (right) for different quantum dot speeds. For the state probability plots, the final probability is labeled in the legend. Cases a) and b) show that for small speeds, the system mostly occupies the two lowest energy orbitals, forming a two-dimensional Hilbert space, as needed for a qubit. However, a higher speed introduces higher excited states and does not behave as a two-level system anymore. The faster the movement, the greater the amplitude of the spatial oscillations. The red line in the probability density plots represent the position of the center of the quantum dot $\xi(t)$.

probability density. Note that these oscillations occur as a consequence of a superposition of eigenstates in which the state probability p is time-independent.

As a consequence, one can interpret the plots of figure 7 as a two-step process. Firstly, when the speed of the quantum dot v_{QD} is above some threshold speed (see appendix A 3 for a derivation of such a threshold speed), the adiabatic approximation becomes invalid. In this non-adiabatic regime, the initial ground state can be written as a superposition of some instantaneous eigenstates with varying state probabilities. At the end of the perturbation (t_1 assuming the trajectory $\xi(t)$ as defined above), provided it was not too strong, the wavefunction can be expressed as a superposition of the two lowest eigenstates of the final Hamiltonian with time-independent state probabilities (hence constant state probabilities in figure 7 after the perturbation). Secondly, this superposition of two eigenstates, which can be seen as equivalent to Rabi oscillations, implies spatial oscillations as shown above.

Note, however, that equation A4 does not account for the evolution of the amplitude of the oscillations with v_{QD} , since this derivation assumes a time-independent Hamiltonian which does not fully describe the simulations of figure 7. It is still possible to derive this equation by looking at the classical equation of motion of a driven harmonic oscillator. Indeed, we show in appendix B that the average position evolution of a driven quantum harmonic oscillator follows the classical equation of motion. This correctly accounts for the oscillations observed in figure 7.

3. Criterion for the transition to the non-adiabatic regime

In this section, we derive a criterion describing the passage from the adiabatic to the non-adiabatic regime for the 1D model. We will drop the time-dependence of ξ to simplify notations, but keep in mind that ξ still correspond to a linear trajectory as defined in equation (1) of the main text. We can expand the Hamiltonian of the 1D model as follows:

$$\hat{H}(t) = \frac{\hat{p}^2}{2m} + \frac{1}{2}m\omega^2\hat{x}^2 + \frac{1}{2}m\omega^2\xi^2 - m\omega^2\xi\hat{x}$$

The derivative with respect to time comes out as:

$$\frac{\partial\hat{H}}{\partial t} = m\omega^2\dot{\xi}(\xi - \hat{x})^2 = -m\omega^2\dot{\xi}(\hat{x} - \xi)^2 \quad (\text{A5})$$

Following the book by Bransden and Joachain [19], the probability amplitude of the first excited state under the adiabatic approximation is (equation 9.100):

$$C_1(t) = \hbar^{-1} \int_{t_0}^t ds \omega^{-1} \left(\frac{\partial\hat{H}}{\partial s} \right)_{1,0} \exp \left(i \int_{t_0}^s \omega du \right)$$

with $\left(\frac{\partial\hat{H}}{\partial s} \right)_{1,0} \equiv \langle \varphi_1(s) | \frac{\partial\hat{H}}{\partial s} | \varphi_0(s) \rangle$ and $\{\varphi_n(t)\}_{n \in \mathbb{N}}$ are the eigenstates of the harmonic oscillator centered at $\xi(t)$. From equation A5 we have:

$$\begin{aligned} \left(\frac{\partial\hat{H}}{\partial s} \right)_{1,0} &= -m\omega^2\dot{\xi} \langle \varphi_1(s) | \hat{x} - \xi(s) | \varphi_0(s) \rangle \\ &= -m\omega^2\dot{\xi} \langle \varphi_1(0) | \hat{x} - \xi(0) | \varphi_0(0) \rangle \end{aligned}$$

Using the generating function for the Hermite polynomials (see equation 4.174 of the book by Bransden and Joachain [19]), one has the following identity:

$$\langle \varphi_n | \hat{x} | \varphi_m \rangle = \begin{cases} \sqrt{\frac{\hbar}{m\omega}} \sqrt{\frac{n}{2}} & \text{if } m = n - 1 \\ \sqrt{\frac{\hbar}{m\omega}} \sqrt{\frac{n+1}{2}} & \text{if } m = n + 1 \\ 0 & \text{else} \end{cases}$$

Hence:

$$\left(\frac{\partial\hat{H}}{\partial s} \right)_{1,0} = -m\omega^2\dot{\xi} \sqrt{\frac{\hbar}{2m\omega}}$$

We can then obtain a more explicit expression for the probability amplitude of the first orbital excited state:

$$\begin{aligned} C_1(t) &= \hbar^{-1} \int_{t_0}^t ds \omega^{-1} \left(\frac{\partial\hat{H}}{\partial s} \right)_{1,0} \exp \left(i \int_{t_0}^s \omega du \right) \\ &= \frac{-m\omega^2}{\hbar\omega} \sqrt{\frac{\hbar}{2m\omega}} \int_{t_0}^t ds \dot{\xi}(s) \exp(i\omega(s - t_0)) \\ &= -\omega \sqrt{\frac{m}{2\hbar\omega}} \int_{t_0}^t ds \dot{\xi}(s) \exp(i\omega(s - t_0)) \end{aligned}$$

At this stage, it is useful to introduce the maximum speed of a quantum harmonic oscillator in the ground state. Assuming that the total energy corresponds to kinetic energy, we have $E_0 = \frac{\hbar\omega}{2} = \frac{1}{2}mv_{\max}^2$, where $v_{\max} \equiv \sqrt{\frac{\hbar\omega}{m}}$ the maximal speed. We can then rewrite the expression for $C_1(t)$ as:

$$C_1(t) = \frac{-\omega}{\sqrt{2}} \int_{t_0}^t ds \frac{\dot{\xi}(s)}{v_{\max}} \exp(i\omega(s - t_0)) \quad (\text{A6})$$

For $t_0 \leq t \leq t_1$, $\dot{\xi}(t) = v_{QD}$ and we can obtain the transition probability from the modulus squared of $C_1(t)$:

$$P_{0 \rightarrow 1}(t) = 2 \left(\frac{v_{QD}}{v_{\max}} \right)^2 \left| \sin \left(\frac{\omega}{2}(t - t_0) \right) \right|^2 \quad (\text{A7})$$

Note that for $t \geq t_1$, $\dot{\xi}(t) = 0$ and the transition probability is constant and equal to $P_1(t_1)$ as expected.

The adiabatic approximation is valid only if at all times the transition probability P_1 is small. In other words, we require $2 \left(\frac{v_{QD}}{v_{\max}} \right)^2 \ll 1$ i.e. $v_{QD} \ll v_{\lim} \equiv \frac{v_{\max}}{\sqrt{2}}$.

In our case, $\Delta E = \hbar\omega = 1$ meV, which gives $v_{\text{lim}} \simeq 22$ nm/ps. Taking 10% of this speed (such that the $(v_{QD}/v_{\text{max}})^2 \ll 1$ criterion is met) gives 2.2 nm/ps, a reasonable delineator between the adiabatic and non-adiabatic regimes, which is of course a smooth transition in reality. Note that this matches the results obtained in the first row of figure 7 where $v_{QD} = 2.5$ nm/ps.

As for the time-dependence of $P_{0 \rightarrow 1}(t)$, note that it is very slow as expected. Indeed, for $\Delta E = \hbar\omega = 1$ meV, the period of oscillations is $T_{0 \rightarrow 1} = \frac{4\pi}{\hbar} \simeq 19$ ps, but the perturbation acts during a time much less than this, so that the probability does not evolve by much.

4. Estimation of the probability of higher excited state

Let us assume the adiabatic condition is met by the linear trajectory ξ , for the 1D model. From equation (4.174) and (9.97) of reference [19], we can estimate that the probability amplitude of the second excited state $C_2(t)$ is related to the amplitude of the first excited state $C_1(t)$ by:

$$\dot{C}_2(t) = \frac{C_1(t)}{\hbar\omega} \left(\frac{\partial \hat{H}}{\partial t} \right)_{2,1} e^{i\omega(t-t_0)}$$

Following the calculation of $\left(\frac{\partial \hat{H}}{\partial t} \right)_{1,0}$ as above, we find that $\left(\frac{\partial \hat{H}}{\partial t} \right)_{2,1} = -m\omega^2 \dot{\xi} \sqrt{\frac{\hbar}{m\omega}}$. Using equation A6 we find:

$$\dot{C}_2(t) = -i\omega \left(\frac{v_{QD}}{v_{\text{max}}} \right)^2 \left(e^{2i\omega(t-t_0)} - e^{i\omega(t-t_0)} \right)$$

Integrating out provides:

$$C_2(t) = 2 \left(\frac{v_{QD}}{v_{\text{max}}} \right)^2 \sin \left(\frac{\omega}{2}(t-t_0) \right)^2 e^{i\omega(t-t_0)}$$

Finally, the transition probability to the second excited state can be computed as:

$$P_{0 \rightarrow 2}(t) = 4 \left(\frac{v_{QD}}{v_{\text{max}}} \right)^4 \left| \sin \left(\frac{\omega}{2}(t-t_0) \right) \right|^4 \quad (\text{A8})$$

Comparing A7 and A8 we see that the probability of the electron being in the second excited state after some time is the square of it being in the first excited state. As we assumed we are in the adiabatic limit, such that the ratio $2 \left(\frac{v_{QD}}{v_{\text{max}}} \right)^2 \ll 1$, and that $0 \leq 4 \left| \sin \left(\frac{\omega}{2}(t-t_0) \right) \right|^4 \leq 4$, then we can expect this transition probability to be vanishingly small. Hence we can expect to remain in a good two-level system whilst in the adiabatic regime. As before, this matches well with our numerical results at low speeds (see the results of figure 7.a for instance where there are no second excited states present.)

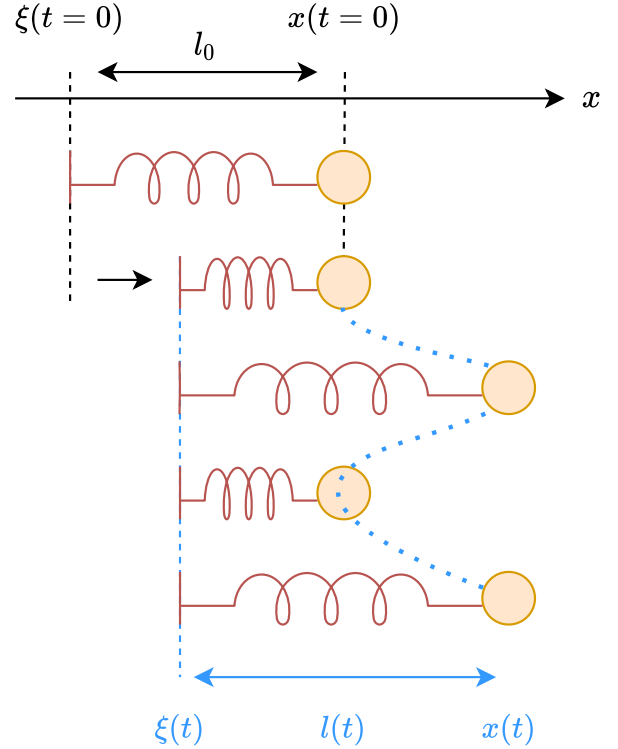


FIG. 8. Schematic of the classical analogy. In this case, the spring is assumed to have been moved faster than the adiabatic limit. We can observe that when the spring is moved, the mass initially stays at the same position - it does not have enough time to react to the external perturbation. As a consequence, this stored spring force will be released, making the mass oscillate at later times.

5. Classical analogy

The results obtained from the 1D simulation are easy to understand using a classical analogy of a mass attached to a spring (see figure 8). The mass represents the electron confined to the quantum dot potential (represented by the spring's own harmonic spring potential). Denote the position of the spring's origin by $\xi(t)$ and the position of the mass by $x(t)$ such that the spring length at rest is given by $l = l_0 = x(t=0) - \xi(t=0)$. Hence, in this analogue, a displacement $\delta\xi$ of the quantum dot potential amounts to moving the origin of the spring ξ . One can picture that if the spring is moved slowly, the length of the spring remains the same through the movement ($l(t) = l_0$), and similarly the mass' trajectory follows suit - as if it were attached by a rigid bar. However, if the spring is pushed quickly, one can expect the spring length to change. This then stores energy in the spring which is subsequently released, causing the mass on the end to start oscillating. Hence the final trajectory of the mass will be a sharp impulse due to the initial perturbation followed by subsequent oscillations.

Let us now show that the average position of the parti-

cle in our experiment obeys the same equation of motion as in the classical case. In the classical case, the spring potential is given by $V(x, t) = \frac{1}{2}m\omega^2(x(t) - \xi(t))^2$. In the quantum case, we need to replace the x variable by the position operator $\hat{x} : |\psi\rangle \mapsto x|\psi\rangle$. Similarly, we replace the function ξ by the operator $\hat{\xi}(t) : |\psi\rangle \mapsto \xi(t)|\psi\rangle$. The potential operator becomes:

$$\begin{aligned}\hat{V} &= \frac{1}{2}m\omega^2(\hat{x} - \hat{\xi}(t))^2 \\ &= \frac{1}{2}m\omega^2\hat{x}^2 + \frac{1}{2}m\omega^2\hat{\xi}^2 - \frac{1}{2}m\omega^2\{\hat{x}, \hat{\xi}\}\end{aligned}$$

where $\{\}$ denotes the anti-commutator. Since $\hat{\xi}$ only multiplies the state by a time-dependent constant, it commutes with the position operator (note that we also have $[\hat{\xi}, \hat{p}] = 0$ since $\xi(t)$ does not depend on x , so is unaffected by the derivative in the momentum operator $\hat{p} = \frac{\hbar}{i}\frac{d}{dx}$). Hence, the potential simplifies and we can write the Hamiltonian of the system as:

$$\hat{H} = \frac{\hat{p}^2}{2m} + \frac{1}{2}m\omega^2\hat{x}^2 + \frac{1}{2}m\omega^2\hat{\xi}(t)^2 - m\omega^2\hat{x}\hat{\xi}(t) \quad (\text{A9})$$

As for any operator \hat{A} :

$$\frac{d\langle\hat{A}\rangle}{dt} = \left\langle \frac{\partial\hat{A}}{\partial t} + \frac{1}{i\hbar} [\hat{A}, \hat{H}] \right\rangle \quad (\text{A10})$$

then by considering the momentum operator provides the following commutators relations:

$$\begin{aligned}\frac{d\langle\hat{p}\rangle}{dt} &= \left\langle \frac{\partial\hat{p}}{\partial t} + \frac{1}{i\hbar} [\hat{p}, \hat{H}] \right\rangle = \left\langle \frac{1}{i\hbar} [\hat{p}, \hat{H}] \right\rangle \\ &= \frac{1}{i\hbar} \left\langle \frac{1}{2}m\omega^2 [\hat{p}, \hat{x}^2] - m\omega^2\xi(t) [\hat{p}, \hat{x}] \right\rangle \\ &= \frac{1}{i\hbar} \left\langle m\omega^2 \frac{-2i\hbar\hat{x}}{2} + m\omega^2\xi(t)i\hbar \right\rangle \\ &= m\omega^2 (\xi(t) - \langle\hat{x}\rangle(t))\end{aligned}$$

Similarly for \hat{x} :

$$\begin{aligned}\frac{d\langle\hat{x}\rangle}{dt} &= \left\langle \frac{\partial\hat{x}}{\partial t} + \frac{1}{i\hbar} [\hat{x}, \hat{H}] \right\rangle = \frac{1}{i\hbar} \langle [\hat{x}, \hat{H}] \rangle \\ &= \frac{1}{i\hbar} \left\langle \frac{2i\hbar\hat{p}}{2m} \right\rangle \\ &= \frac{\langle\hat{p}\rangle}{m}\end{aligned}$$

By taking the derivative with respect to time we have that:

$$\frac{d^2\langle\hat{x}\rangle}{dt^2} = \frac{1}{m} \frac{d\langle\hat{p}\rangle}{dt} = \omega^2 (\xi(t) - \langle\hat{x}\rangle(t))$$

This last equality can be viewed as the equation of a classical harmonic oscillator driven by some external excitation $\xi(t)$, namely:

$$\frac{d^2\langle\hat{x}\rangle}{dt^2} + \omega^2\langle\hat{x}\rangle = \omega^2\xi(t) \quad (\text{A11})$$

Hence we see that the average position behaves exactly as in the classical case of a driven harmonic oscillator. In particular, this proves that the spatial oscillations depend only on the potential parameter ω and not on the initial conditions. This also justifies our observations concerning the evolution of the amplitude of the oscillations with the speed of the quantum dot: for a classical harmonic oscillator, a greater initial speed induces a greater amplitude of oscillation.

Appendix B: Methods

To solve Schrodinger's equation the Crank-Nicolson method was used. The results of the first section were also reproduced using a time-dependent perturbation theory approach.

As a further validation of our modelling, we simulated the experiment from *Yamahata et al.* using only the Hamiltonian \mathcal{H}_x of equation (2) and obtained similar probability densities.

For the valley-orbit model, the onsite energy parameter ϵ of Boykin's model was adjusted to 1.4 eV such that the obtained spectrum had negative values close to zero. This allowed for easier differentiating between 'real' eigenvectors and "artificial" eigenvectors whose eigenvalue of 0 is purely induced by the addition of defects (these were added by setting the column and row of the concerned lattice site to zero in the Hamiltonian). The difference between our chosen value of ϵ and Boykin's choice [9] was then restored in the plot describing the time evolution of the spectrum. The values used for the off-diagonal elements can be found in figure 2 of reference [9].

To implement the interface steps, we first constructed Boykin's Hamiltonian for N_z atoms with N_z being the initial width of the quantum well. With some basic trigonometry, we can compute how many atoms are required at each position x for a given miscut angle. We set the onsite energy and the hopping terms from/to of all the atoms falling outside the domain to zero, effectively imposing hard-wall boundary conditions.

[1] B. Kaestner and V. Kashcheyevs, Non-adiabatic quantized charge pumping with tunable-barrier quantum dots:

a review of current progress, Reports on Progress in

- Physics **78**, 103901 (2015).
- [2] G. Yamahata, S. Ryu, N. Johnson, H.-S. Sim, A. Fujiwara, and M. Kataoka, Picosecond coherent electron motion in a silicon single-electron source, *Nature Nanotechnology* **14**, 1019–1023 (2019).
- [3] F. A. Zwanenburg, A. S. Dzurak, A. Morello, M. Y. Simmons, L. C. L. Hollenberg, G. Klimeck, S. Rogge, S. N. Coppersmith, and M. A. Eriksson, Silicon quantum electronics, *Reviews of Modern Physics* **85**, 961–1019 (2013).
- [4] D. Culcer, A. L. Saraiva, B. Koiller, X. Hu, and S. Das Sarma, Valley-based noise-resistant quantum computation using si quantum dots, *Physical Review Letters* **108**, 10.1103/physrevlett.108.126804 (2012).
- [5] P. Boross, G. Széchenyi, D. Culcer, and A. Pályi, Control of valley dynamics in silicon quantum dots in the presence of an interface step, *Physical Review B* **94**, 10.1103/physrevb.94.035438 (2016).
- [6] D. Kim, Z. Shi, C. B. Simmons, D. R. Ward, J. R. Prance, T. S. Koh, J. K. Gamble, D. E. Savage, M. G. Lagally, M. Friesen, and et al., Quantum control and process tomography of a semiconductor quantum dot hybrid qubit, *Nature* **511**, 70–74 (2014).
- [7] J. Schoenfield, B. Freeman, and H. Jiang, Coherent manipulation of valley states at multiple charge configurations of a silicon quantum dot device, *Nat Commun* **8**, 10.1038/s41467-017-00073-x (2017).
- [8] N. Penthorn, J. Schoenfield, and J. e. a. Rooney, Two-axis quantum control of a fast valley qubit in silicon, *npj Quantum Information* **5**, 10.1038/s41534-019-0212-5 (2019).
- [9] T. B. Boykin, G. Klimeck, M. Friesen, S. N. Coppersmith, P. von Allmen, F. Oyafuso, and S. Lee, Valley splitting in low-density quantum-confined heterostructures studied using tight-binding models, *Phys. Rev. B* **70**, 165325 (2004).
- [10] R. Rahman, J. Verduijn, N. Kharche, G. P. Lansbergen, G. Klimeck, L. C. L. Hollenberg, and S. Rogge, Engineered valley-orbit splittings in quantum-confined nanostructures in silicon, *Physical Review B* **83**, 10.1103/physrevb.83.195323 (2011).
- [11] M. Friesen and S. N. Coppersmith, Theory of valley-orbit coupling in a si/sige quantum dot, *Physical Review B* **81**, 10.1103/physrevb.81.115324 (2010).
- [12] M. Friesen, S. Chutia, C. Tahan, and S. N. Coppersmith, Valley splitting theory of sige si sige quantum wells, *Physical Review B* **75**, 10.1103/physrevb.75.115318 (2007).
- [13] T. B. Boykin, G. Klimeck, M. A. Eriksson, M. Friesen, S. N. Coppersmith, P. von Allmen, F. Oyafuso, and S. Lee, Valley splitting in strained silicon quantum wells, *Applied Physics Letters* **84**, 115–117 (2004).
- [14] B. Tariq and X. Hu, Effects of interface steps on the valley-orbit coupling in a si/sige quantum dot, *Physical Review B* **100**, 10.1103/physrevb.100.125309 (2019).
- [15] D. Culcer, X. Hu, and S. Das Sarma, Interface roughness, valley-orbit coupling, and valley manipulation in quantum dots, *Physical Review B* **82**, 10.1103/physrevb.82.205315 (2010).
- [16] D. L. Campbell, Y.-P. Shim, B. Kannan, R. Winik, D. K. Kim, A. Melville, B. M. Niedzielski, J. L. Yoder, C. Tahan, S. Gustavsson, and et al., Universal nonadiabatic control of small-gap superconducting qubits, *Physical Review X* **10**, 10.1103/physrevx.10.041051 (2020).
- [17] H. R. L. Jr. and W. B. Riesenfeld, An exact quantum theory of the time-dependent harmonic oscillator and of a charged particle in a time-dependent electromagnetic field 10.1063/1.1664991 (1969).
- [18] M. C. Bertin, B. M. Pimentel, and J. A. Ramirez, Construction of dynamical invariants for the time-dependent harmonic oscillator with a time-dependent driven force (2014), arXiv:1409.2429 [math-ph].
- [19] C. J. J. B. H. Bransden, *Quantum mechanics*, 2nd edition, (2000).